Materials Today Chemistry 8 (2018) 29–35

Contents lists available at ScienceDirect

Materials Today Chemistry

journal homepage: www.journals.elsevier.com/materials-today-chemistry/

Cysteamine-modified ZIF-8 colloidal building blocks: Direct assembly of nanoparticulate MOF films on gold surfaces via thiol chemistry

Gustavo M. Segovia [a, b], Jimena S. Tuninetti [a], Sergio Moya [d], Agustín S. Picco [a, c], Marcelo R. Ceolín [a], Omar Azzaroni [a, *], Matías Rafti [a, **]

[a] Instituto de Investigaciones Fisicoquímicas Teóricas y Aplicadas (INIFTA), Fac. de Cs. Exactas, Universidad Nacional de La Plata – CONICET, 64 y Diag. 113, 1900 La Plata, Argentina
[b] Universidad Nacional de San Martin, Argentina
[c] Laboratório Nacional de Nanotecnologia (LNNano)/Laboratório Nacional de Luz Síncrotron (LNLS), Centro Nacional de Pesquisa em Energia e Materiais (CNPEM), CEP 13083-970, Caixa Postal 6192, Campinas, SP, Brazil
[d] CIC biomaGUNE, Parque Científico y Tecnológico de Gipuzkoa, Paseo Miramón 182, 20014 Donostia/San Sebastián, Gipuzkoa, Spain

ARTICLE INFO

Article history:
Received 26 November 2017
Received in revised form
30 January 2018
Accepted 2 February 2018

Keywords:
Metal organic frameworks (MOFs) colloidal suspensions
Films self-assembly
ZIF-8 microporous films
Cysteamine modification
SAXS/WAXS

ABSTRACT

Chemical modification of metal organic framework (MOF) nanocrystal colloids was used to endow them with chemical affinity for gold substrates. Modified nanocrystals were then used as building blocks for rapid and selective self-assembly of porous films. Cysteamine (Cys, 2-aminoetanethiol) was chosen as both chemical modulator and functionalizing agent of Zeolite Imidazolate Framework-8 (ZIF-8) MOF nanocrystals. Important parameters such as the impact of the modulator on the range of nanocrystals stability, size, polydispersity, morphology, and crystalline structure were assessed *via* both, small and wide angle x-ray scattering (SAXS and WAXS). Cysteamine modified ZIF-8 nanocrystals were assembled into films over conductive Au substrates and film growth was followed *in-situ* with Quartz Crystal Microbalance (QCM). Thiol moieties exposed out of the ZIF-8 surface after cysteamine modification, results in the formation of thiol bonds with Au conductive substrates as shown via Cyclic Voltammetry experiments. The strategy here presented allows for the synthesis of pre-designed building blocks for MOF films on metal surfaces.

1. Introduction

Microporous Coordination Polymers, also known as Metal Organic Frameworks (MOFs), are an emerging class of microporous crystalline materials composed of metal nodes (or clusters containing metals) coordinated with polydentate organic ligands [1–6]. The nature of interactions enabling supramolecular assembly of the nanometer-sized MOF units, and the properties of such assemblies, can be tuned *via* modification of both their surface chemistry and morphology [7–9]. This fact has been recognized some time ago, and several examples can be found in the literature, where both structural and chemical flexibility of MOFs were exploited in order to create interesting new composite materials [10–12]. A great part of MOFs appeal, results from the multiple possible combinations between metal centers and organic ligands, leading to a continuously increasing number of applications; e.g., separations [13–16], catalysis [17,18], biomedicine [19–21], electrochemistry, energy conversion/storage [22–24], and greenhouse-effect capture agents [25,26]. MOF films offer a new playground for the creation of "smart" surfaces, which rely on the use of *ad-hoc* modifications intended to confer a desired functionality [27–29]. For example, the enhancement of structure-based molecular interactions (e.g., charge, size, geometry), or chemical functionality [30], allows the controlled release of a molecular cargo in drug-delivery applications [31], or an increased catalytic activity [32]. In particular, the assembly of MOF films over conductive substrates results in a great variety of new electroactive surfaces with interesting differential properties, given that both chemical and mechanical stability are ensured [33–36]. When films are constructed by substrate dip-coating using colloidal suspensions of MOF nanocrystals; both, intrinsic microporosity given by its internal crystalline structure, and mesoporosity arising from spatial arrangement of individual building units are present. This strategy has proved to be suitable for controlling film permeation properties, as recently explored [37,38].

* Corresponding author.
** Corresponding author.
E-mail addresses: azzaroni@inifta.unlp.edu.ar (O. Azzaroni), mrafti@quimica.unlp.edu.ar (M. Rafti).

https://doi.org/10.1016/j.mtchem.2018.02.002
2468-5194/

Taking into account these concepts, we have employed surface modified MOFs crystals for film growth. Having in mind the strong affinity between sulfur and gold [39,40], we have synthesized colloidal suspensions of ZIF-8 MOF nanocrystals, and after proper modification with a thiol, we used them as building blocks for porous films grown over conductive Au substrates. ZIF-8 was selected given both its straightforward synthesis, long time stability near-neutral pH, and intrinsic microporosity [30,41,42]. This member of a MOF subclass known as Zeolitic Imidazolate Frameworks (ZIFs), can be described as an infinite sodalite (SOD) topology network of Zn^{2+} metallic centers tetrahedrally coordinated with bidentate 2-methylimidazolate (2-Hmim) organic linkers [43]. Cysteamine was employed as modifier to provide chemical affinity to the nanocrystals for conductive gold substrates through the expected thiol moieties exposed on the outer surface of the MOF nanocrystal after functionalization. Cysteamine can readily coordinate Zn^{+2}, as demonstrated by the great variety of amino-complexes reported [44]. However, cysteamine was also found to be responsible for concentration -and time- dependent morphological changes in the nanocrystals. A partial “roughening” of the otherwise smooth nanocrystal surface and even a total loss of ZIF-8 structure could be observed depending on time and molar proportions used. Our experiments show that direct cysteamine modification of ZIF-8, when performed within a suitable concentration range, enables the assembly of ZIF-8+Cys nanocrystals into stable films linked to Au surfaces.

2. Materials and methods

2.1. Reagents and synthesis

Different concentrations of ZIF-8 precursors and cysteamine were used to assess the effect on nanoparticle size and polydispersity of the colloidal suspensions obtained. Cysteamine ideally provides a surface modified colloidal suspension of nanocrystals decorated with thiol moieties; however, a suitable concentration range for such modification must be determined due to the possible instability of Zn^{2+} metal centers towards cysteamine coordination. The reagents used during the synthesis and surface modification were; methanol (CH_3OH Anedra, RA-ACS), zinc nitrate hexahydrate ($ZnNO_3 \cdot 6H_2O$ Sigma Aldrich 98%), 2-methylimidazole ($C_4H_6N_2$ Aldrich 99%), and cysteamine (C_2H_7NS Acros Organics 98%). The procedures followed to synthesize and functionalize ZIF-8 colloidal suspensions are summarized in the Supporting Information. Briefly, ZIF-8 and cysteamine modified ZIF-8 (ZIF-8+Cys) films were deposited *via* simple room temperature dip coating of clean Au substrates with MOF colloidal suspensions as above stated. Film growth was *in-situ* followed *via* Quartz Crystal Microbalance with Dissipation (QCMD), and time required for final state was determined in each case. Colloidal ZIF-8 nanocrystals suspensions were synthesized using different volumes of 25 mM zinc nitrate, and 50 mM 2-methylimidazole methanolic mother solutions, according to the targeted precursor molar ratio. The time needed to attain final state of the colloidal ZIF-8 nanocrystals suspensions was approx. 40 min, as determined using time resolved Dynamic Light Scattering (DLS) and turbidity measurements. For cysteamine modification, different volumes of cysteamine methanolic mother solution were used, depending on the targeted molar ratios.

2.2. Cysteamine modification and ZIF-8 stability range determination

UV–Visible modular spectrometer Ocean Optics 4000 UV–Vis was used to obtain the ZIF-8 stability range with Cys. UV–Vis measurements were performed in the wavelength interval ranging from 400 to 800 nm, where neither ZIF-8 nanocrystals suspension, nor its precursors or Cys feature absorption bands. In this way, any absorbance baseline increase detected for mixtures of ZIF-8 precursors can be directly attributed to nanocrystal scattering. Following such procedure, time resolved ZIF-8 nanocrystals growth, and suitable molar ratios for successful cysteamine functionalization were determined. A Varian – 660-IR apparatus equipped with ATR accessory was used in order to characterize the obtained materials.

2.3. Characterization of nanocrystals via dynamic light scattering

In-situ DLS experiments were performed using a Zetasizer Nano ZS apparatus from Malvern, to determine nanocrystal colloids size distribution and polydispersity.

2.4. X-ray wide and small angle scattering

Size distributions, polydispersity, and shape of colloidal suspensions were assessed using small angle X-ray scattering (SAXS), while crystalline structure was studied using wide angle X-ray scattering (WAXS) on dry samples. The SAXS/WAXS system (INIFTA, project “Nanopymes”, EuropeAid/132184/D/SUP/AR-Contract 331-896) is a XEUSS 1.0 HR (XENOCS, Grenoble) equipped with a microfocus X-ray source and a Pilatus 100 K detector (DECTRIS AG, Switzerland), which allow both solid and liquid phase measurements in a temperature controlled cell.

2.5. Transmission electron microscopy

Transmission Electron Microscopy (TEM) was used for morphology characterization. Images were obtained with a LaB6-TEM of type JEOLJEM-1400PLUS (40 kV–120 kV) equipped with a GATAN US1000 CCD camera (2 k × 2 k).

2.6. Scanning electron microscopy

Scanning Electron Microscopy (SEM) technique was used in order to characterize nanocrystal morphology. Images were acquired using a FEI Quanta 200 apparatus.

2.7. Characterization of chemical composition via X-ray photoelectron spectroscopy (XPS)

XPS experiments were performed in a SPECS Sage HR 100 spectrometer with a non-monochromatic X-ray source (Aluminium Kα line of 1486.6 eV energy and 300 W), placed perpendicular to the analyzer axis and calibrated using the $3d_{5/2}$ line of Ag with a full width at half maximum (FWHM) of 1. Measurements were carried out after purification of the synthesized MOF nanoparticles by centrifugation and fresh solvent wash, in an iterative way, in order to remove precursors and cysteamine moieties that would introduce misleading signals if still present in the sample.

2.8. Film growth in-situ measurements via quartz crystal microbalance (QCM) and E-QCM

Measurements were performed on a quartz microbalance from Q-Sense, Gothenburg, Sweden. The equipment has a chamber with an 80 μL volume, which is closed at one side by the quartz crystal. The cell can be filled and the fluid exchanged using the standard Q-Sense flow system. Quartz crystals, purchased from Q-sense, have a main resonance frequency at 5 MHz. For applications in electrochemistry, an analog output proportional to frequency shift may be directly connected to a potentiostat. The potentiostat digitizes the

voltage, and its software displays relative frequency changes synchronous with the electrochemical data.

2.9. AFM

AFM was performed with a Veeco Multimode atomic force microscope attached to a Nanoscope V controller to image the modified gold substrates.

3. Results and discussion

3.1. ZIF-8 colloidal suspension modification with cysteamine

Fig. 1 show results obtained for the time evolution of turbidity after direct mixing of ZIF-8 precursors, and subsequent addition of cysteamine to a final high molar ratio. Recent examples of procedures directed to obtain chemically modified MOFs, use nearly-equimolar ratios between linker and modifier agent [45–47]; however, due the high affinity between cysteamine and ZIF-8, much lower modifying agent molar ratios were needed. In Fig. 1 it can be clearly observed, from the turbidity increase the formation of ZIF-8 colloidal suspension, which rapidly decrease after adding cysteamine solution for a final molar proportion (metal: linker: cys) of *1:2:1.5* at $t = 400$ s (see S.I. for details, and video file in which total disassembly of ZIF-8 nanocrystals is presented). The stability range for ZIF-8 nanocrystal colloidal suspensions was systematically tested for progressively lower molar proportions of cysteamine modulator, yielding the $1{:}2{:}8 \times 10^{-4}$ M proportion as maximum suitable proportion for successful modification (i.e., when a higher than $1{:}2{:}8 \times 10^{-4}$ M proportion is used, a total disassembly rather than surface functionalization occurs).

Supplementary video related to this article can be found at https://doi.org/10.1016/j.mtchem.2018.02.002.

3.2. Small angle X-ray scattering

In order to evaluate the effect of cysteamine modification and molar proportions of precursors on size, shape, and polydispersity of colloidal ZIF-8 nanocrystals obtained, *in-situ* SAXS experiments were carried. Fig. 2 shows data obtained and fits performed on scattering patterns of the samples analyzed are summarized in Table 1. Two different precursor proportions with and without cysteamine (ZIF-8 and ZIF-8+Cys) were tested. Molar proportions used for precursors were (metal: linker) = (*1:2*) and (*1:10*), while cysteamine molar proportion was kept to ($1{:}8 \times 10^{-4}$) (metal: Cys) (see S.I. for further details). A hard sphere model [48], implemented in the freely available SasView software (v. 2.2.0. at sasview.org), was fitted to the experimental data. Polydispersity index (PDI) was taken into account applying Gaussian distribution of radii. Remarkably, within the range of synthesis conditions explored, the colloidal system develops a size distribution which allows the observation of intensity minima expected for hard spheres SAXS patterns. A decrease in size and a PDI increase are observed when molar proportion of linker was increased. Further reduction in size and increase in PDI can also be observed when cysteamine modulator is added for fixed (metal: linker) molar proportions. These results are also in line with DLS experiments carried using even higher linker molar proportions (see S.I.). According to previous reports, the observed decrease in particle size could be rationalized in terms of a competing interaction between cysteamine and 2-Hmim linker [47]. Additionally, cysteamine can interfere in the acid/base equilibrium of 2-Hmim; i.e., deprotonation equilibriums of 2-Hmim, which are crucial for the availability of N-bidentate linker constituting the ZIF-8 MOF structure motif [49]. This would in turn affect nucleation and growth mechanism,

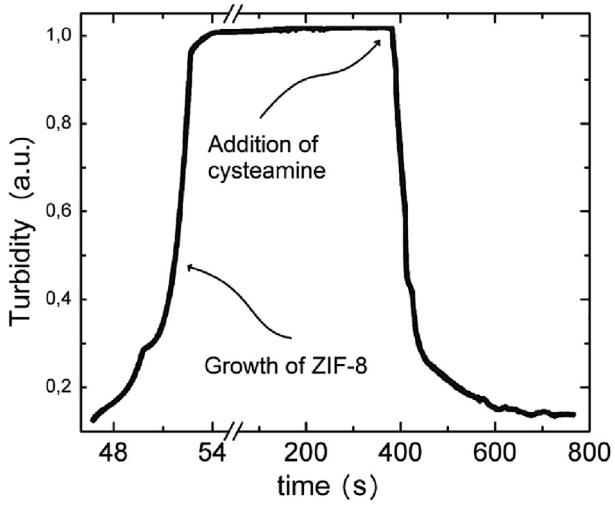

Fig. 1. Evaluation of ZIF-8 nanocrystal colloid formation, and its stability towards modification with cysteamine. Precursors molar proportions used were (metal: linker) = (1:2), and cysteamine was added to the colloidal suspension to achieve a final (metal: linker: Cys) proportion of (1:2:1.5). After Cys addition, turbidity decreases quickly owing to an almost complete ZIF-8 nanocrystals disassembly.

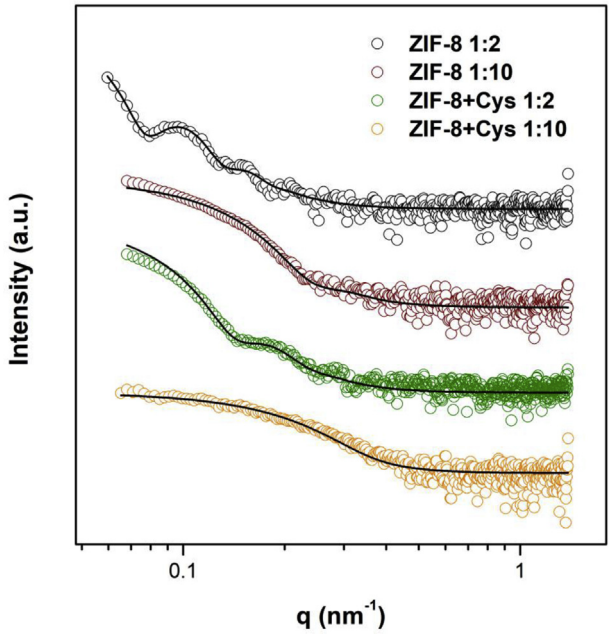

Fig. 2. SAXS scattering patterns of the obtained colloidal suspensions. From top to bottom: **(black)** ZIF-8 molar ratio (*1:2*); **(maroon)** ZIF-8 molar ratio (*1:10*); **(green)** ZIF-8+Cys molar ratio (*1:2*); **(orange)** ZIF-8+Cys molar ratio (*1:10*). In each case, solid line represents hard spheres fit.

Table 1
Fitting parameters corresponding to the SAXS patterns presented in Fig. 2.

Sample	Radius (r, nm)	PDI (δ/r)
ZIF-8 1:2	55.8	0.115
ZIF-8 1:10	16.1	0.208
ZIF-8+Cys 1:2	29.1	0.169
ZIF-8+Cys 1:10	6.47	0.483

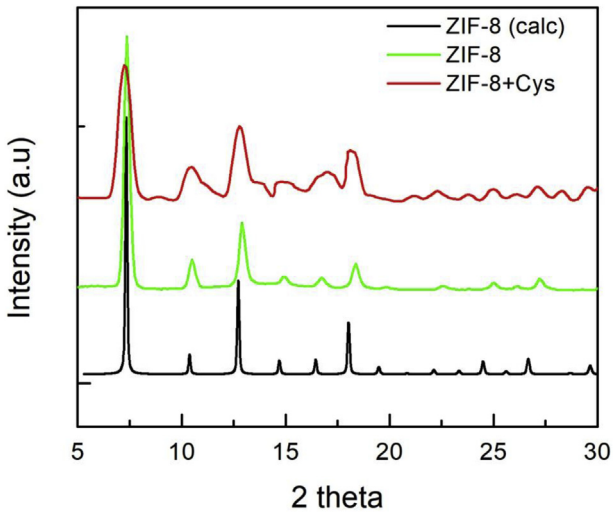

Fig. 3. Powder WAXS patterns obtained from dried ZIF-8 (green) and ZIF-8+Cys (red) colloidal suspensions compared to the calculated ZIF-8 diffractogram (black).

which finally determine size distribution and PDI, *via* formation of $[Zn(2\text{-Hmim})_mL_n]$ complexes in early stages of ZIF-8 formation, with $m > n$, where 2-Hmim is the protonated monodentate linker and L is cysteamine modulator. Such intermediate species, and further deprotonation and linker exchange reactions, would explain the smaller size of nanocrystals obtained. Additional characterization was conducted through ATR-FTIR spectroscopy, ZIF-8 and cysteamine modified ZIF-8 show characteristic vibrational (data not shown; see S.I. for more details).

3.3. Wide angle X-ray scattering – WAXS

Fig. 3 shows powder WAXS experimental patterns for ZIF-8, and ZIF-8+Cys, together with calculated diffractogram from reported structure (obtained using Mercury software) [42,50]. The correspondence between peaks confirms that bulk ZIF-8 crystalline structure, which corresponds to the symmetry space group I-43 m, remains present after cysteamine addition (differences in the diffractograms can be understood taking into account coordinative interactions between metal centers and modifying agent, which were observed to cause the appearance of a "surface roughness" as evidenced in TEM experiments, see below).

3.4. Transmission electron microscopy – TEM

In order to further analyze the effect of chemical modulation, we have exposed the as-obtained ZIF-8 nanocrystal colloid corresponding to the molar ratio (*1:2*) (metal: linker) to cysteamine for a final molar proportion of ($1{:}8 \times 10^{-4}$) (metal: Cys). In good agreement with SAXS fit presented above, TEM images from Fig. 4a and c show characteristic ZIF-8 nanocrystals with ≈50 nm radius.

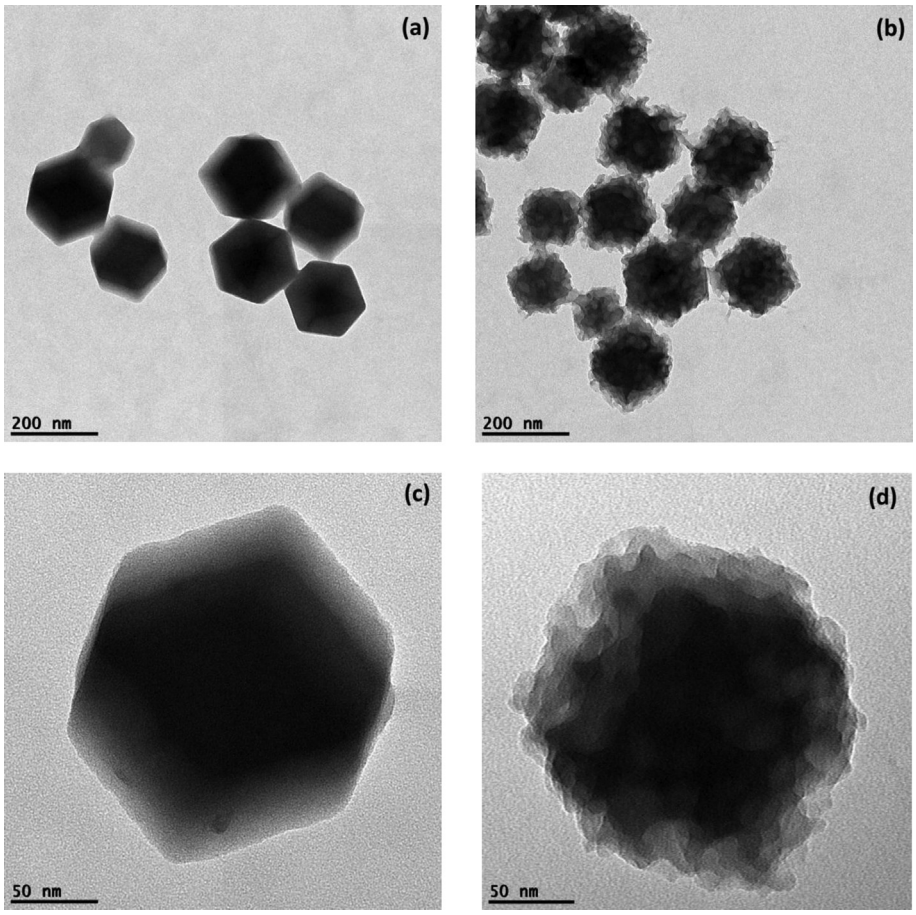

Fig. 4. TEM images showing morphology changes in ZIF-8 nanoparticles after contact with cysteamine. (a) and (c) before cysteamine contact; (b) and (d) after contact. Molar ratio of (metal: linker) precursors was set to (*1:2*), while cysteamine molar proportion was set to ($1{:}8 \times 10^{-4}$) (metal: Cys).

Interestingly, post-synthesis exposure to cysteamine, a clear morphology change can be observed, a "roughening" on the otherwise smooth nanocrystal edges (see Fig. 4b and d).

3.5. X-ray photoelectron spectroscopy – XPS

Surface chemistry of ZIF-8 modified with cysteamine was characterized by XPS. Fig. 5 displays the high resolution XPS spectral region for C *1s*, N *1s*, Zn *2p* and S *2p* for ZIF-8 after cysteamine modification, were characteristic S signals from cysteamine coordination were expected to appear. As can be observed, values founded for C *1s*, Zn *2p* and N *1s* agree well with previously reported XPS binding energies peaks for ZIF-8 [51]. Furthermore, a broad peak is found in the S *2p* region, which confirms the crystallite modification.

This broad peak could be explained having in consideration the tendency towards oxidation of sulfur species (featuring thus, binding energies around 161 eV) [52], and the peaks arising from coordination with Zn in the ZIF-8 nanocrystal surface [44]. This observation allows us to hypothesize on the modulating agent effect; i.e., to yield monodisperse thiol-functionalized ZIF-8 nanocrystals (see S.I. for XPS complete binding energy surveys for both samples).

3.6. Film growth from cysteamine-modified ZIF-8 nanocrystals, characterization of thiol-mediated assembly on Au

3.6.1. Quartz crystal microbalance (QCM) experiments of in-situ film growth and atomic force microscopy (AFM)

Growth profiles of films over conductive Au-coated QCM sensors were obtained using both ZIF-8 and ZIF-8+Cys nanocrystal colloids, as displayed in Fig. 6.

QCM sensor was exposed to colloidal suspensions using a flow-cell, and after reaching constant Δf value; i.e. final stage of assembly, the suspension was replaced with fresh solvent. Differences for both, initial growth speed and final states can be observed, being the deposition of ZIF-8+Cys much faster. Moreover, plateau frequency values obtained for ZIF-8+Cys are approximately 2000 Hz, while Δf for ZIF-8 is less than 800 Hz. Most important, when ZIF-8 films assembled are washed away with fresh solvent, frequency returns to zero initial value immediately; on the other hand, for ZIF-8+Cys films, the same procedure yields a non-zero final frequency of 120 Hz (this being approx. one order of magnitude higher than bare cysteamine assembled monolayers). It can be concluded from these experiments that the assembly of ZIF-8+Cys produces a stable film that cannot be removed in the same fashion as non-modified ZIF-8, being this compatible with the existence of strong nanocrystal-Au interactions arising from thiol moieties. Fig. 7 shows AFM images obtained from different areas on the QCM-D sensor after ZIF-8+Cys film formation, confirming the presence of nanocrystal agglomerates covering substrate surface.

3.6.2. Cyclic voltammetry – CV of synthesized films assembled

Cyclic voltammetry experiments were performed on ZIF-8+Cys assembled films over Au substrates in order to obtain further evidence of thiol-mediated binding. Fig. 8 shows characteristic electrodesorption signal typical for thiol chemisorbed on gold surface [53]. These signals were compared with self-assembled bare cysteamine monolayers (Cys-SAMs) on gold. Taking into account the influence of oxygen reduction, which appears in similar potential range, experiments were performed using inert nitrogen atmosphere (see S.I. for more details). CV experiments performed on Cys-SAMs display two reduction peaks at −0.78 V and −0.97 V (see Fig. 8a), and only for the first cycle, which denotes complete

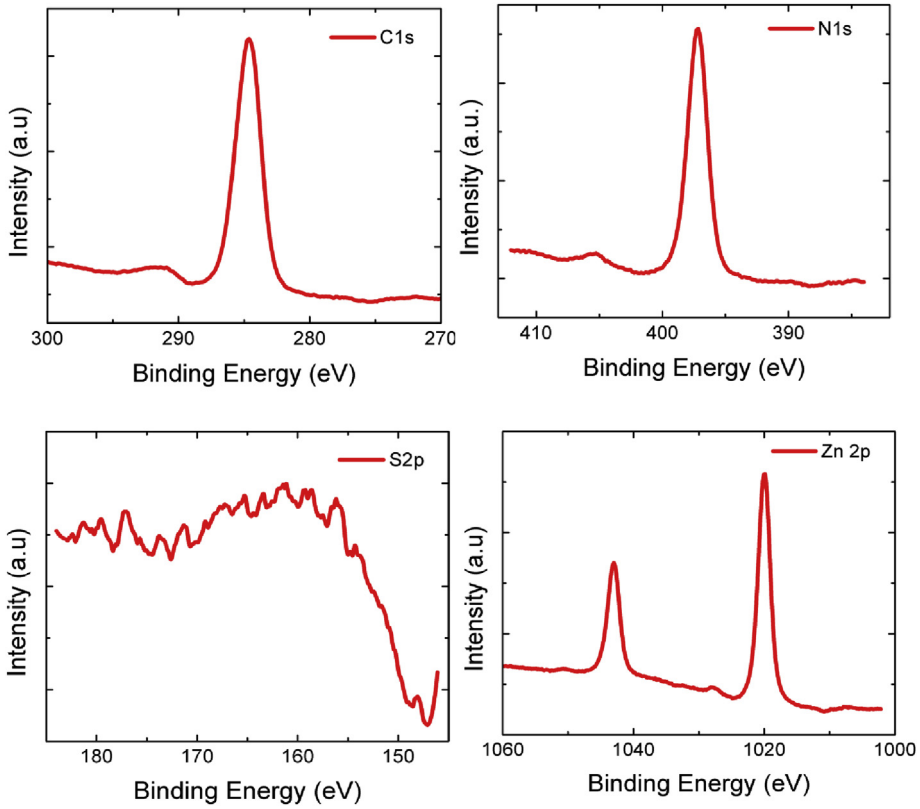

Fig. 5. XPS experiments performed on ZIF-8+Cys nanocrystals showing binding energy regions corresponding to C, Zn, N and S. Sulfur characteristic peaks are only present when cysteamine modification was carried out.

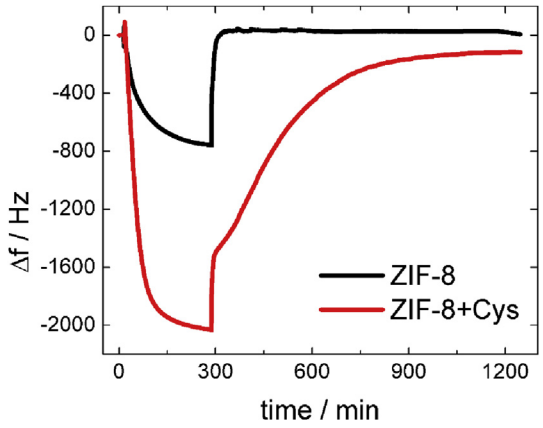

Fig. 6. QCMD frequency changes associated with the time evolution of films grown using ZIF-8 and ZIF-8+Cys nanocrystal colloids. The presence of thiol-moieties changes both initial growth dynamics and final states after fresh solvent washing.

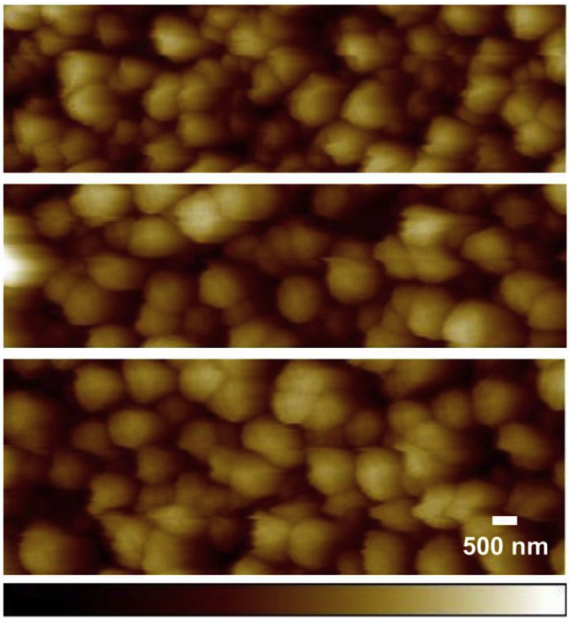

Fig. 7. AFM images obtained from different areas on the assembled ZIF-8+Cys film over Au substrate. Bottom height reference bar color code; 0 nm (black) – 800 nm (white).

electrodesorption. On the other hand, for ZIF-8+Cys films, reduction peaks are shifted to slightly more positive potentials; −0.45 V and −0.80 V, and still appear in the second and third cycles, as shown in Fig. 8b).

The two different electroreduction signals found for each film can be attributed to both, the heterogeneity of the substrate surface, and different order domains in the film, which causes variations in packing density affecting the reduction potentials of adsorbed thiols, as already reported in the literature [53]. The presence of adsorbed species after the first cycle, which is observed for ZIF-8+Cys films, can be understood considering the multiple binding sites provided by thiol moieties exposed on nanocrystal surface, together with the much slower diffusion after electrodesorption compared to the small and mobile cysteamine molecule.

4. Conclusions

We have explored the use of cysteamine as modulator agent for ZIF-8 MOF nanocrystals in colloidal suspensions, and identified suitable molar proportions for efficient surface modification as a general strategy towards conferring them affinity for a given desired surface. Cysteamine allows positioning thiol moieties on the nanocrystal surface *via* competing coordination of Zn^{2+} metal centers, and on the other hand, affects the size distribution and polydispersity of colloidal suspension obtained. The affinity of cysteamine for metal centers is such, that using near to equimolar proportions (Cys: 2-Hmim) ratio, ZIF-8 colloidal suspensions are not stable. The correspondence between powder WAXS patterns of pure and Cys-modified ZIF-8 nanocrystals allows us to hypothesize that crystalline (and thus intrinsic microporosity) structure is not affected to a great extent. However, the morphology suffers modifications as can be observed *via* electron microscopy through a "roughening" of the otherwise smooth nanocrystals surface. XPS experiments allow detection of cysteamine, and suggest that thiol moieties are present on the nanocrystal surface. The presence of surface exposed thiol moieties explain the gained affinity of the nanocrystals for gold substrates, as demonstrated via Quartz Crystal Microbalance, where it was proved that the ZIF-8+Cys form a stable monolayer on gold substrates. Electrodesorption reduction signals corresponding to thiol were observed during cyclic voltammetry experiments, thus confirming the stable nature of ZIF-8+Cys nanocrystal bond to Au surface. We envision that this strategy could be used with minor adaptations for a wide variety of MOFs and surfaces, allowing for quick and straightforward self-assembly of predefined building units with different size in order to create thickness-controlled films with micro and mesoporosity.

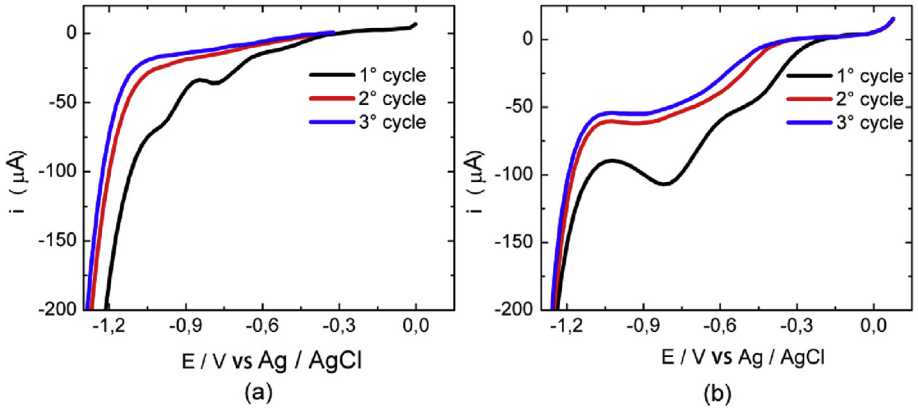

Fig. 8. Voltammograms of; (a) cysteamine self-assembled monolayer, and (b) film assembled from ZIF-8+Cys nanocrystals.

Author contributions

The manuscript was written through contributions of all authors. All authors have given approval to the final version of the manuscript. All authors contributed equally.

Acknowledgments

This work was supported by ANPCyT (PICT- 2013-0905 and PICT-2016-1680), CONICET (PIP 11220130100370CO) Fundación Petruzza, Austrian Institute of Technology GmbH (AIT– CONICET Partner Lab: "Exploratory Research for Advanced Technologies in Supramolecular Materials Science" — Exp. 4947/11, Res. No. 3911, 28-12-2011), and the Marie Curie International Research Staff Exchange Scheme (IRSES) project HIGRAPHEN (Grant No. 612704). J.S.T., A.S.P., M.R.C., O.A. and M.R. are CONICET fellows. G. M. Segovia thanks CONICET for a doctoral fellowship A.S.P. thanks FAPESP for a postdoctoral fellowship (Grant No. 2014/21910-8).

References

[1] B. Hoskins, R. Robson, J. Am. Chem. Soc. 111 (1989) 5962–5964.
[2] O.M. Yaghi, H. Li, C. Davis, D. Richardson, T.L. Groy, Acc. Chem. Res. 31 (1998) 474–484.
[3] H. Li, M. Eddaoudi, M. O'Keeffe, O.M. Yaghi, Nature 402 (1999) 276–279.
[4] J.L.C. Rowsell, O.M. Yaghi, Microporous Mesoporous Mater. 73 (2004) 3–14.
[5] G. Férey, Chem. Soc. Rev. 37 (2008) 191–214.
[6] J.R. Long, O.M. Yaghi, Chem. Soc. Rev. 38 (2009) 1213–1214.
[7] B.W. Jacobs, R.J.T. Houk, M.R. Anstey, S.D. House, I.M. Robertson, A.A. Talin, M.D. Allendorf, Chem. Sci. 2 (2011) 411.
[8] T.R. Cook, Y.R. Zheng, P.J. Stang, Chem. Rev. 113 (2013) 734–777.
[9] D. Bradshaw, S. El-Hankari, L. Lupica-Spagnolo, Chem. Soc. Rev. 43 (2014) 5431–5443.
[10] N. Stock, S. Biswas, Chem. Rev. 112 (2012) 933–969.
[11] I. Ahmed, S.H. Jhung, Mater. Today 17 (2014) 136–146.
[12] A. Zimpel, T. Preiß, R. Röder, H. Engelke, M. Ingrisch, M. Peller, J.O. Rädler, E. Wagner, T. Bein, U. Lächelt, S. Wuttke, Chem. Mater. 28 (2016) 3318–3326.
[13] E.D. Bloch, W.L. Queen, R. Krishna, J.M. Zadrozny, C.M. Brown, J.R. Long, Science (80-) 335 (2012) 1606–1610.
[14] J.R. Li, J. Sculley, H.C. Zhou, Chem. Rev. 112 (2012) 869–932.
[15] K.A. Cychosz, R. Ahmad, A.J. Matzger, Chem. Sci. 1 (2010) 293.
[16] X. Zhang, Y. Liu, S. Li, L. Kong, H. Liu, Y. Li, W. Han, K.L. Yeung, W. Zhu, W. Yang, J. Qiu, Chem. Mater. 26 (2014) 1975–1981.
[17] J. Gascon, A. Corma, F. Kapteijn, F.X. Llabrs, I. Xamena, ACS Catal. 4 (2014).
[18] C. Wang, J. Tuninetti, Z. Wang, C. Zhang, R. Ciganda, L. Salmon, S. Moya, J. Ruiz, D. Astruc, J. Am. Chem. Soc. 139 (2017) 11610–11615.
[19] P. Horcajada, T. Chalati, C. Serre, B. Gillet, C. Sebrie, T. Baati, J.F. Eubank, D. Heurtaux, P. Clayette, C. Kreuz, J.-S. Chang, Y.K. Hwang, V. Marsaud, P.-N. Bories, L. Cynober, S. Gil, G. Férey, P. Couvreur, R. Gref, Nat. Mater. 9 (2010) 172–178.
[20] K. Liang, R. Ricco, C.M. Doherty, M.J. Styles, S. Bell, N. Kirby, S. Mudie, D. Haylock, A.J. Hill, C.J. Doonan, P. Falcaro, Nat. Commun. 6 (2015) 7240.
[21] P. Horcajada, R. Gref, T. Baati, P.K. Allan, G. Maurin, P. Couvreur, G. Férey, R.E. Morris, C. Serre, Chem. Rev. 112 (2012) 1232–1268.
[22] W. Liu, X.-B. Yin, TrAC Trends Anal. Chem. 5 (2015) 9269.
[23] Y. Han, P. Qi, S. Li, X. Feng, J. Zhou, H. Li, S. Su, X. Li, B. Wang, Chem. Commun. (Camb) 60 (2014) 8057–8060.
[24] D. Wu, Z. Guo, X. Yin, Q. Pang, B. Tu, L. Zhang, Y.G. Wang, Q. Li, Adv. Mater. 26 (2014) 3258–3262.
[25] K. Sumida, D.L. Rogow, J.A. Mason, T.M. McDonald, E.D. Bloch, Z.R. Herm, T.H. Bae, J.R. Long, Chem. Rev. 112 (2012) 724–781.
[26] G. Férey, C. Serre, T. Devic, G. Maurin, H. Jobic, P.L. Llewellyn, G. De Weireld, A. Vimont, M. Daturi, J.-S. Chang, Chem. Soc. Rev. 40 (2011) 550–562.
[27] D. Zacher, O. Shekhah, C. Wöll, R.A. Fischer, Chem. Soc. Rev. 38 (2009) 1418.
[28] P. Horcajada, C. Serre, D. Grosso, C. Boissière, S. Perruchas, C. Sanchez, G. Férey, Adv. Mater. 21 (2009) 1931–1935.
[29] A. Bétard, R.A. Fischer, Chem. Rev. 112 (2012) 1055–1083.
[30] G. Lu, J.T. Hupp, J. Am. Chem. Soc. 132 (2010) 7832–7833.
[31] O. Azzaroni, S.E. Moya, A.A. Brown, Z. Zheng, E. Donath, W.T.S. Huck, Adv. Funct. Mater. 16 (2006) 1037–1042.
[32] M. Rafti, A. Brunsen, M.C. Fuertes, O. Azzaroni, G.J.A.A. Soler-Illia, ACS Appl. Mater. Interfaces 5 (2013) 8833–8840.
[33] H.K. Arslan, O. Shekhah, J. Wohlgemuth, M. Franzreb, R.A. Fischer, C. Wöll, Adv. Funct. Mater. 21 (2011) 4228–4231.
[34] O. Shekhah, Materials (Basel) 3 (2010) 1302–1315.
[35] M. Rafti, J.A. Allegretto, G.M. Segovia, J.S. Tuninetti, J.M. Giussi, E. Bindini, O. Azzaroni, Mater. Chem. Front. 1 (2017) 2256–2260.
[36] J. Cravillon, S. Münzer, S.J. Lohmeier, A. Feldhoff, K. Huber, M. Wiebcke, Chem. Mater. 21 (2009) 1410–1412.
[37] J.S. Tuninetti, M. Rafti, O. Azzaroni, RSC Adv. 5 (2015) 73958–73962.
[38] M. Rafti, W.A. Marmisollé, O. Azzaroni, Adv. Mater. Interfaces 3 (2016) 1600047.
[39] J.C. Love, L.A. Estroff, J.K. Kriebel, R.G. Nuzzo, G.M. Whitesides, Chem. Rev. 105 (2005) 1103–1169.
[40] O. Azzaroni, M.E. Vela, H. Martin, A. Hernández Creus, G. Andreasen, R.C. Salvarezza, Langmuir 17 (2001) 6647–6654.
[41] B. Wang, A.P. Côté, H. Furukawa, M. O'Keeffe, O.M. Yaghi, Nature 453 (2008) 207–211.
[42] O. Karagiaridi, M.B. Lalonde, W. Bury, A.A. Sarjeant, O.K. Farha, J.T. Hupp, J. Am. Chem. Soc. 134 (2012) 18790–18796.
[43] K.S. Park, Z. Ni, A.P. Cote, J.Y. Choi, R. Huang, F.J. Uribe-Romo, H.K. Chae, M. O'Keeffe, O.M. Yaghi, Proc. Natl. Acad. Sci. 103 (2006) 10186–10191.
[44] H. Fleischer, Y. Dienes, B. Mathiasch, V. Schmitt, D. Schollmeyer, Inorg. Chem. 44 (2005) 8087–8096.
[45] A.F. Gross, E. Sherman, J.J. Vajo, Dalt. Trans. 41 (2012) 5458.
[46] M.C. McCarthy, V. Varela-Guerrero, G.V. Barnett, H.K. Jeong, Langmuir 26 (2010) 14636–14641.
[47] J. Cravillon, R. Nayuk, S. Springer, A. Feldhoff, K. Huber, M. Wiebcke, Chem. Mater. 23 (2011) 2130–2141.
[48] A. Guinier, G. Fournet, Small-angle scattering of X-rays, John Wiley and Sons, Inc., New York, NY, 1955.
[49] L. Riauba, G. Niaura, O. Eicher-Lorka, E. Butkus, J. Phys. Chem. A 110 (2006) 13394–13404.
[50] I.J. Bruno, J.C. Cole, P.R. Edgington, M. Kessler, C.F. Macrae, P. McCabe, J. Pearson, R. Taylor, Acta Crystallogr. Sect. B Struct. Sci. 58 (2002) 389–397.
[51] R.L. Papporello, E.E. Miró, J.M. Zamaro, Microporous Mesoporous Mater. 211 (2015) 64–72.
[52] M. Wirde, U. Gelius, L. Nyholm, Langmuir 15 (1999) 6370–6378.
[53] T. Kawaguchi, H. Yasuda, K. Shimazu, M.D. Porter, Langmuir 16 (2000) 9830–9840.